Direct measurement of the Hall effect in a free-electron-like surface state

Toru Hirahara, Iwao Matsuda,* Canhua Liu, Rei Hobara, Shinya Yoshimoto, and Shuji Hasegawa
Department of Physics, School of Science, University of Tokyo, 7-3-1 Hongo, Bunkyo-ku, Tokyo 113-0033, Japan
(Received 22 March 2006; published 19 June 2006)

We have succeeded in directly measuring the Hall effect in a single-atomic layer on a Si(111) crystal surface. Our four-point-probe transport measurements under magnetic field showed that the behavior of majority carriers in the surface state changed from electronlike to holelike during the structural conversion from the $\sqrt{3}\times\sqrt{3}$-Ag to $\sqrt{21}\times\sqrt{21}$-(Ag,Au) surface superstructure. This is due to a change in the Fermi surface caused by band folding. The results are discussed quantitatively and shown to be consistent with the electronic structure obtained by photoemission spectroscopy.

DOI: 10.1103/PhysRevB.73.235332 PACS number(s): 73.20.−r, 73.25.+i, 73.63.−b, 79.60.Dp

I. INTRODUCTION

The Hall effect, since its discovery in 1879, has been one of the most important topics in solid-state physics[1] because it is very useful for determining the type, concentration, and mobility of majority carriers in specimens. Furthermore, it is also used as a tool to explore peculiar properties in low-dimensional physics. For example, the anomalous Hall effect is used for characterizing magnetism of diluted magnetic semiconductors.[2] The integer and fractional quantum Hall effects have been found in two-dimensional electron systems in semiconductor heterostructures,[3,4] which are possibly the best-studied platforms for many-body physics. Recently, there have been a number of reports on the Hall effect and magnetoresistance at metal or metal silicide ultrathin films on semiconductor substrates, showing exotic phenomena, such as an oscillation in sign of the Hall coefficient with film thickness.[5–8] However, up to now, there has been no experimental report on the Hall effect in a monatomic layer, i.e., in a surface state that is characteristic of the topmost atomic layer of a crystal. By using such an *atomically thin two-dimensional electron gas* (2DEG) system composed of free-electron-like surface states, here we report the measurement of the Hall effect and present a change in the behavior of majority carriers by adsorption of electron donor adatoms on the surface. Such characterization of monolayer transport properties has general interest not only for the category of low-dimensional physics, but also for applications in nanoscience and nanotechnology.

We have employed the Si(111)$\sqrt{3}\times\sqrt{3}$-Ag surface ($\sqrt{3}$-Ag, in short, hereafter) as the sample, which is known from photoemission spectroscopy (PES) to have an isotropic, parabolic, free-electron-like surface state [Fig. 1(g)], i.e., an atomic layer with a 2DEG system.[9–12] As shown in Figs. 1(a) and 1(c), its Fermi surface (ring) is a complete circle (electron pocket) centered at the $\bar{\Gamma}$ point in the $\sqrt{3}\times\sqrt{3}$-surface Brillouin zone (SBZ). By depositing monovalent dopant adatoms, such as noble- or alkali-metal atoms on the surface, the electron pocket becomes larger because electrons are doped into the band.[11] The adatoms (e.g., Au) sit on specific sites on the surface and, at a certain coverage (~0.14 monolayer), a new ordered phase, $\sqrt{21}\times\sqrt{21}\pm R10.89°$ ($\sqrt{21}$-(Ag,Au), in short, hereafter), is created. The circular Fermi surface for this superstructure is larger than the $\sqrt{21}\times\sqrt{21}$-SBZ as shown in Figs. 1(b) and 1(d).[9] From the area in k-space, in total three valence electrons are estimated to exist in the $\sqrt{21}\times\sqrt{21}$ unit cell;[12] two of the three fully occupy the first SBZ, and the remaining one partially occupies the second and third SBZs. As described in textbooks on solid-state physics,[13] due to Bragg reflection at the boundaries of the

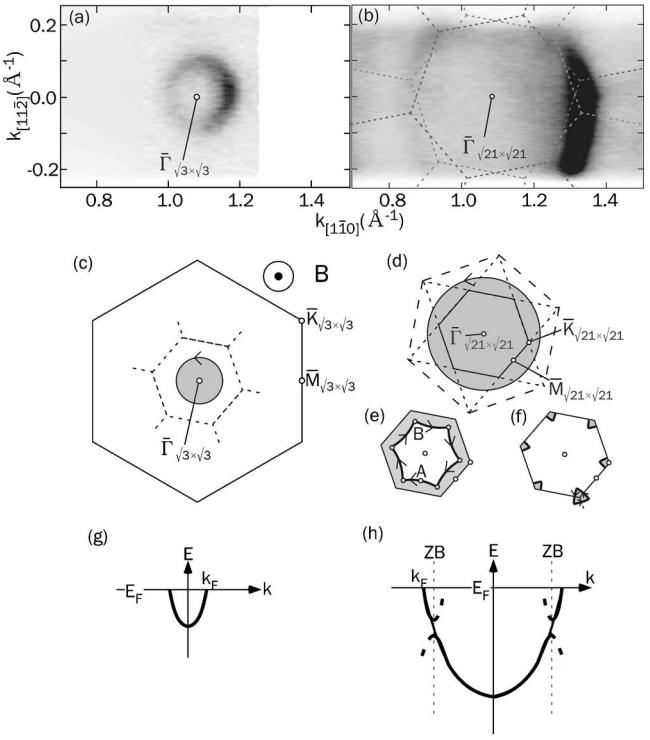

FIG. 1. (a,b) The photoemission intensity maps at the Fermi level (Fermi surface) measured for the $\sqrt{3}$-Ag (a) and $\sqrt{21}$-(Ag,Au) (b) surfaces. For a comparison, the dotted lines in (b) indicate the double domain $\sqrt{21}\times\sqrt{21}$ SBZ boundaries. (c) Schematic drawing of a free-electron-like Fermi surface of the $\sqrt{3}$-Ag. The dotted lines indicate one of the $\sqrt{21}\times\sqrt{21}$ SBZs. (d) The Fermi surface of the $\sqrt{21}$-(Ag,Au) in the extended SBZ scheme, and (e) in the second and (f) third SBZs in the reduced SBZ scheme. The shaded area represents electron-filled regions.[9] The arrows on the Fermi surface indicate the motion of Fermi electrons under a magnetic field (B) out of the paper. (g,h) Schematic drawing of the change of the free-electron-like surface-state band due to the structure transformation from $\sqrt{3}$-Ag (g) to $\sqrt{21}$-(Ag,Au) (h).

Brillouin zone, the bands and Fermi surface should be folded and viewed in the reduced zone scheme. The surface-state band no longer forms a simple electron pocket as shown in Fig. 1(h), with a gap formed at the zone boundary. As a result of this band folding, a hole pocket appears around the $\bar{\Gamma}$ point in the reduced second SBZ [Fig. 1(e)], while small electron pockets are formed at the $\bar{K}$ point in the third SBZ [Fig. 1(f)].[9]

When a magnetic field (B) is applied perpendicular to the surface, carriers move along the Fermi surface in k-space.[13] When B is in the direction pointing out of the paper as in Fig. 1(c), the electrons in the $\sqrt{3}$-Ag surface state take a counterclockwise orbit (an electronlike orbit). On the other hand, for the $\sqrt{21}$-(Ag,Au), the electrons take a large clockwise orbit (a holelike orbit) in the second SBZ [Fig. 1(e)] and a small counterclockwise orbit (an electronlike orbit) in the third SBZ [Fig. 1(f)]. This means that the majority carriers in the surface state of $\sqrt{21}$-(Ag,Au) should behave as holes because there are much more carriers in the second SBZ than in the third SBZ. In other words, *the majority carrier in the surface state should change from electronlike to holelike* by the structural conversion from the $\sqrt{3}$-Ag to $\sqrt{21}$-(Ag,Au). Since the Hall coefficient R_H is expressed as

$$R_H = -\frac{1}{e(N_n - N_p)} \text{ (high-field limit)} \tag{1}$$

$$R_H = -\frac{N_n - N_p}{e(N_n + N_p)^2} \text{ (low-field limit)}, \tag{2}$$

where $N_{n(p)}$ is the concentration of carriers behaving electron(hole)like, R_H of the surface-state carriers should be negative for the $\sqrt{3}$-Ag and positive for the $\sqrt{21}$-(Ag,Au). Actually from the measured Fermi surfaces in Fig. 1(a), we can estimate the electron density at the $\sqrt{3}$-Ag to be $N_n = 1.6\times10^{13}$ cm^{-2}, giving $R_H = -39\ \Omega\ \mathrm{T}^{-1}$ by Eq. (2). Since, from Fig. 1(b), the hole (electron) density in the second (third) SBZ of the $\sqrt{21}$-(Ag,Au) surface is similarly estimated to be $N_p = 4.3\times10^{13}$ cm^{-2} ($N_n = 0.4\times10^{13}$ cm^{-2}), in total $R_H = +11\ \Omega\ \mathrm{T}^{-1}$ by Eq. (2).

On the other hand, it has been one of the difficulties in the previous macroscopic four-point probe method to extract the surface-state conductivity value, which is typically hidden in the contributions from the bulk and surface space-charge layer.[14] However, by focusing on the *change* of the measured conductivity, the contribution from the bulk can be ignored and the surface-state contribution can be extracted by considering the change of the space-charge layer, as described in detail later. The surface space-charge layer at the subsurface region, which is induced by band bending, is known to be a p-type accumulation layer for the $\sqrt{3}$-Ag, but a depletion layer for the $\sqrt{21}$-(Ag,Au).[14] As a consequence, through the $\sqrt{3}$-Ag–to–$\sqrt{21}$-(Ag,Au) conversion, N_p should decrease and R_H should become larger in the surface space-charge layer. This occurs irrespective whether the substrate Si crystal is n-type or p-type. However, since this change is opposite to that in the surface state (N_p increases and R_H changes from negative to positive), it enables us to distinguish the contribution from the surface state and that from the space-charge layer.

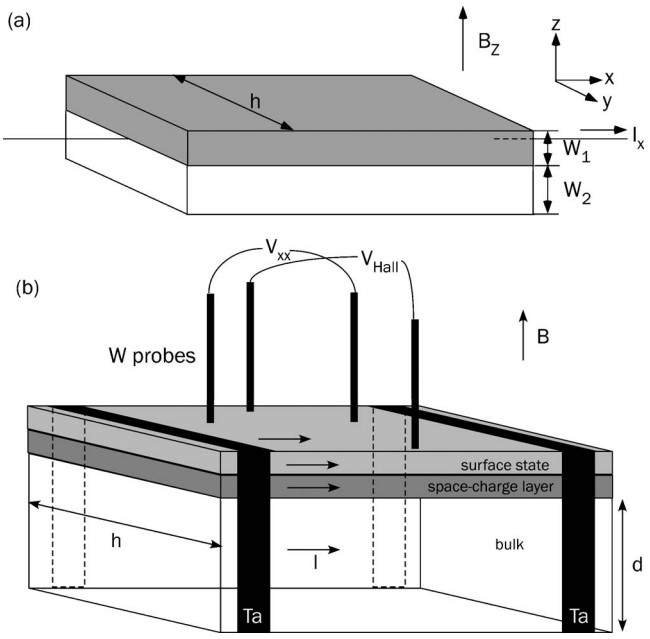

FIG. 2. (a) Schematic drawing of the two-layer model, in the form of two parallel slabs, to mimic a nonuniform sample in the surface-normal direction. These layers, for example, represent two channels through the surface state and surface space-charge layer. (b) Schematic drawing of the experimental setup in the present measurement with the silicon wafer, tantalum(Ta) clamps and tungsten(W) wire-contact electrodes.

In this study, we found that the experimentally obtained positive Hall coefficient R_H of the $\sqrt{21}$-(Ag,Au) was smaller than that of the $\sqrt{3}$-Ag. This means that the number of carriers exhibiting holelike behavior has increased. As described above, this change is opposite to that expected from the surface space-charge layer and consistent with that expected for the surface state. Furthermore, from the quantitative analysis based on the two-layer model,[15] the results of Hall effect and conductivity are consistent with those expected from the transformation of the Fermi surface described in Fig. 1. It means that surface-state magnetotransport measurements can be successfully explained by the band structure obtained by photoemission spectroscopy.

II. EXPERIMENTAL

The experiment was performed using the *in situ* macroscopic four-point probe method in ultrahigh vacuum (UHV).[16] We extended the technique to Hall-effect measurements by applying a surface-normal magnetic field up to 6 T. The four probes of tungsten (W) wires (0.3 mm diam) for measuring the voltage drops were just pressed on the sample surface in an arrangement as shown in Fig. 2(b) before installing the sample holder in the UHV chamber. The current was made to flow between the two tantalum (Ta) clamps at both ends, and we simultaneously measured the longitudinal voltage (V_{xx}) and Hall voltage (V_{Hall}) with the magnetic field

at room temperature. The probe spacings were 8 and 3 mm for the longitudinal and Hall voltages, respectively. We used both *p*-type (*B*-doped, 3900–6400 Ω cm) and *n*-type (*P*-doped, 1–10 Ω cm) of Si(111) wafers (0.5 mm thick). After flashing the sample at 1250 °C, we obtained a clear 7×7 reflection high-energy electron diffraction (RHEED) pattern. The $\sqrt{3}$-Ag surface was prepared by one monolayer (ML) Ag deposition on the clean Si(111)7×7 surface at 500 °C, and the $\sqrt{21}$-(Ag,Au) was formed by subsequent ~0.14 ML Au deposition on the $\sqrt{3}$-Ag at room temperature[10,17] (1 ML$=7.83\times10^{14}$ atoms/cm^2).

By irradiating the RHEED beam to the vicinity of the probe contacts, we could obtain information about the surface structure there, which actually showed some difference from the structure at the central part of wafer. Such degradation of surface structures near the probe contacts may be due to contamination from the probe wires, shadowing effect on the evaporated beam by the probe wire, and/or lower temperature only near the contact points at flashing heating. However, since the size of such degraded areas at the vicinity of probe contacts, about 0.1 mm wide, is much smaller than the probe spacing, typically 8–10 mms, the measured results are basically not affected. In the four-point probe method, the voltage probes do not need to directly contact the $\sqrt{3}$-Ag or $\sqrt{21}$-(Ag,Au) region because the distribution of equipotential lines along the sample surface (and also in the depth direction) between the voltage probes are not affected by the voltages probes themselves. This is because no current essentially flows through the voltage probes. Therefore, the situation at the probe contacts does not affect the results. This is a great advantage of the four-point probe method.[16,18]

III. THEORY

We first discuss the current distribution in a three-dimensional inhomogeneous sample as depicted in Fig. 2(a), the so-called two-layer model.[15] We assume two layers whose thicknesses are W_1 and W_2, and the carrier density and/or the mobility are different in the two layers. These layers correspond to the surface state and surface space-charge layer, for example. They can be regarded as parallel conductors, meaning that the electric field along the surface-parallel direction is the same for both layers. We want to know the relation between the measured conductivity and the Hall coefficient (σ, R_H) and those of the individual layers ($\sigma_1,\sigma_2,R_{H1},R_{H2}$). The definition of σ and R_H in a homogeneous sample are

$$\sigma=\frac{J_x}{E_x}=\frac{I_x}{hWE_x}, \tag{3}$$

$$R_H=\frac{E_y}{B_zJ_x}=\frac{hWE_y}{B_zI_x}, \tag{4}$$

respectively, where the current flows along the x direction (I_x) and the magnetic field is applied along the z direction (B_z). h and $W(=W_1+W_2)$ are the width and thickness of the sample. From the above definitions, we obtain

$$R_H\sigma^2=\frac{E_y}{E_x^2}\frac{I_x}{hWB_z}. \tag{5}$$

First, we derive the relation for the conductivity using Eq. (3). As we assume that the inhomogeneous sample consists of parallel conductors, the sum of the current flowing in the upper layer I_{x1} and that in the lower I_{x2} should equal that flowing as a whole($I_{\mathrm{tot}}=I_{x1}+I_{x2}$). Therefore, we obatin

$$\sigma_1=\frac{I_{x1}}{hW_1E_x} \tag{6}$$

$$\sigma_2=\frac{I_{x2}}{hW_2E_x} \tag{7}$$

$$\sigma=\frac{I_{x1}+I_{x2}}{h(W_1+W_2)E_x}, \tag{8}$$

and

$$(W_1+W_2)\sigma=W_1\sigma_1+W_2\sigma_2. \tag{9}$$

For the Hall coefficient, we use Eq. (5). Similar treatement to the above case results in the following equations:

$$R_{H1}\sigma_1^2=\frac{E_y}{E_x^2}\frac{I_{x1}}{hW_1B_z}, \tag{10}$$

$$R_{H2}\sigma_2^2=\frac{E_y}{E_x^2}\frac{I_{x2}}{hW_2B_z}, \tag{11}$$

$$R_H\sigma^2=\frac{E_y}{E_x^2}\frac{I_{x1}+I_{x2}}{h(W_1+W_2)B_z}. \tag{12}$$

Finally, we obtain

$$(W_1+W_2)R_H\sigma^2=W_1R_{H1}\sigma_1^2+W_2R_{H2}\sigma_2^2. \tag{13}$$

Since in our measurement geometry shown in Fig. 2(b), the wire and clamp electrodes contact, electrically, both the surface state and the substrate, the measuring current flows along three channels in parallel: (i) the surface state having conductivity σ_{ss} and Hall coefficient R_{Hss}, (ii) the surface space-charge layer (σ_{sc},R_{Hsc}), and (iii) the interior bulk (σ_b,R_{Hb}).[14] The quantities for the surface state and the space-charge layer are two dimensional values $\sigma^{2\mathrm{D}}=W\sigma$, $R_H^{2\mathrm{D}}=R_H/W$ in Eq. (3) and (4), respectively. The above two-layer model (multilayer in this case) can be applied in the present case.[15] Changing Eq. (9) and (13) to the two-dimensional case using σ and R_H in two-dimensions (sheet conductivity and sheet Hall coefficient), we obtain

$$\sigma=\sigma_{ss}+\sigma_{sc}+d\sigma_b, \tag{14}$$

$$R_H\sigma^2=R_{Hss}\sigma_{ss}^2+R_{Hsc}\sigma_{sc}^2+dR_{Hb}\sigma_b^2, \tag{15}$$

where d is the thickness of the wafer. Although the bulk component is dominant among the three terms in the right-hand sides of Eqs. (14) and (15), σ_b and R_{Hb} do not change even if the surface structure changes. Therefore, the measured *changes* between different surface structures on the same wafer can be related by

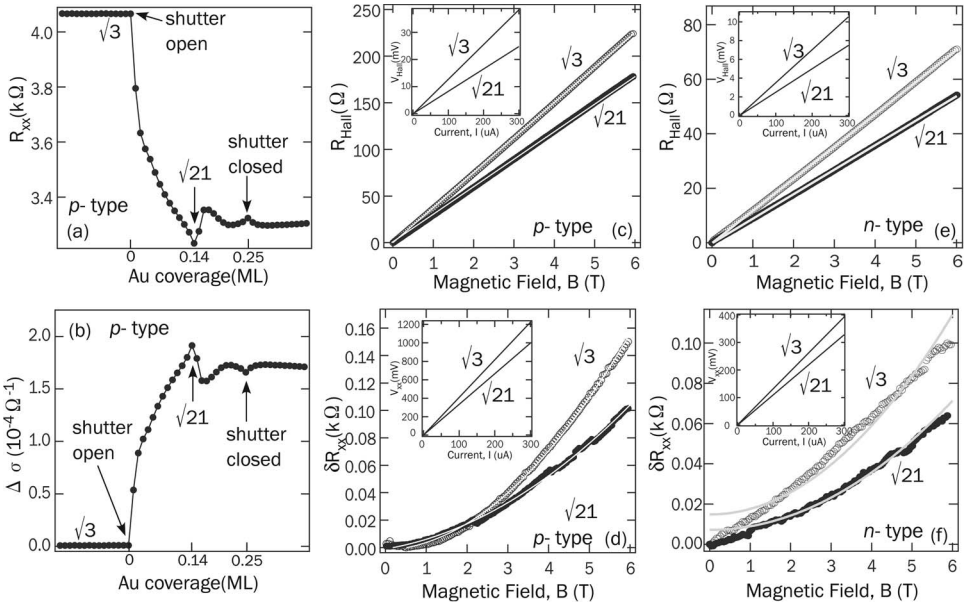

FIG. 3. (a,b) The longitudinal resistance ($R_{xx}=V_{xx}/I$) (a) and the change of the sheet conductivity ($\Delta\sigma$) (b) measured as a function of Au coverage on the $\sqrt{3}$-Ag at RT. The $\sqrt{21}$-(Ag,Au) surface, indicated by $\sqrt{21}$, is formed around 0.14 ML Au coverage. (c–f): The Hall resistance ($R_{\mathrm{Hall}}=V_{\mathrm{Hall}}/I$) (c,e) and the change of longitudinal resistance [δR_{xx} in Eq. (18)] (d,f) measured as a function of the magnetic field for the $\sqrt{3}$-Ag (open circles) and $\sqrt{21}$-(Ag,Au) surfaces (closed circles). The data were taken with *p*-(*B*-doped, 3900–6400 Ω cm) (c,d) and *n*-(*P*-doped, 1–10 Ω cm) type Si(111) wafers (e,f). The insets show the current-voltage (*I-V*) curves at 3 T (c,e) and at 0 T (d,f), respectively.

$$\Delta\sigma = \Delta\sigma_{ss} + \Delta\sigma_{sc}, \tag{16}$$

$$\Delta(R_H\sigma^2) = \Delta(R_{Hss}\sigma_{ss}^2) + \Delta(R_{Hsc}\sigma_{sc}^2). \tag{17}$$

Next we calculate the changes of the space-charge layer components $\Delta\sigma_{sc}$, $\Delta(R_{Hsc}\sigma_{sc}^2)$ by solving the Poisson equation; the band bending value is known from PES, giving the carrier density there.[14] Finally, the changes of the surface-state components $\Delta\sigma_{ss}$ and $\Delta(R_{Hss}\sigma_{ss}^2)$ can be derived by subtracting the space-charge layer contributions from the measured changes. In the present study, we could not measure the absolute values of R_{Hss} for lack of accuracy and sensitivity in the macroscopic four-probe measurements. We only focus on the change $\Delta(R_{Hss}\sigma_{ss}^2)$ caused by the structural transformation from the $\sqrt{3}$-Ag to $\sqrt{21}$-(Ag,Au) in this study. This is enough for knowing the behavior of majority carriers in the surface states.

IV. RESULTS AND DISCUSSION

Figure 3(a) shows the change of the resistance during Au deposition on the $\sqrt{3}$-Ag surface for the *p*-type Si wafer. As is obviously seen, the $\sqrt{21}$-(Ag,Au) has a lower resistance (higher conductivity) than the $\sqrt{3}$-Ag. The increase in sheet conductivity is $\Delta\sigma \sim 1.5\times10^{-4}\ \Omega^{-1}$ [Fig. 3(b), Table I], which is similar to those of the previous studies.[14] The inset in Fig. 3(d) shows the measured current-voltage (*I-V*) curves, showing clear ohmic behaviors.

Figures 3(c) and 3(e) show the Hall resistance, R_{Hall} measured as a function of the magnetic field for the two surfaces on the *p*- and *n*-type wafers, respectively. The inset shows current-Hall voltage curves measured at 3 T, which again shows ohmic behavior. The Hall resistance ($R_{\mathrm{Hall}}=R_HB$) has increased linearly with magnetic field as shown by the overlapped white straight lines.[19] The gradient ($=R_H$) of the fitted straight lines is positive for both surfaces, and the value is larger for $\sqrt{3}$-Ag than for the $\sqrt{21}$-(Ag,Au).[20] The results are summarized in Table I.[20] From the definition of R_H, this clearly indicates *the increase in carrier density behaving as holes* by the $\sqrt{3}$-to-$\sqrt{21}$ conversion. This is *an unambiguous detection of the Hall effect of carriers in the surface state* because, as mentioned in the Introduction, an opposite change in R_H is expected from the carriers in the surface space-charge layer.

Figures 3(d) and 3(f) show the change of the longitudinal resistance $R_{xx}(=V_{xx}/I)$ when the magnetic field is changed, which exhibits a nearly parabolic dependence. According to the estimation of carrier relaxation time τ,[9,10] the value of $\omega_c\tau=(eB/m^*)\tau$ at $B=6$ T is ~0.05 for the surface states and ~0.24 for the silicon bulk states. Therefore, this parabolic dependence is due to the fact that our measurement was performed in the low-field limit ($\omega_c\tau \ll 1$) and R_{xx} can be fitted by[21]

$$\frac{\delta R_{xx}}{R_{xx}(B=0)} = \frac{R_{xx}(B)-R_{xx}(B=0)}{R_{xx}(B=0)} = \xi\mu_H^2B^2, \tag{18}$$

where μ_H is the Hall mobility of carriers and ξ is a constant governed by the scattering mechanism of carriers ($\xi \sim 0.273$ for acoustic phonon scattering, which is dominant at room temperature[21]). From the curve-fit in Fig. 3(d), we can estimate μ_H values as shown by μ_H (2) in Table I. On the other hand, the values of Hall mobility $\mu_H(=R_H\sigma)$ calculated from the experimental values of R_H and σ are also listed as μ_H (1) in Table I. These values are of the same order of magnitude as the hole mobility in the bulk Si crystal ($\mu=480\ \mathrm{cm^2/Vs}$).[21,22] Therefore, it means that the present macroscopically measured results contain conductivity of the surface to a certain degree although those of the bulk and space-charge layer are dominant. But as described above, we can extract the surface contributions by focusing on the *differences* in R_{xx} and R_{Hall} between the two surface structures.

TABLE I. The upper columns show the measured values of sheet conductivity σ and Hall coefficient R_H, and $R_H\sigma^2$ for the $\sqrt{3}$-Ag and $\sqrt{21}$-(Ag,Au) surfaces obtained using $p(3900-6400\ \Omega\,\mathrm{cm})$- and $n(1-10\ \Omega\,\mathrm{cm})$-type Si substrates in the present four-point probe and Hall-effect measurements. The differences between the two surfaces, $\Delta\sigma$ and $\Delta(R_H\sigma^2)$ are also listed. The Hole mobility $\mu_H(1)$ calculated from R_H and σ, and $\mu_H(2)$ calculated from the magnetic-field dependence of R_{xx} [Eq. (18)] are also listed. The experimental error is estimated to be about 15%. The numerically calculated values by solving the Poisson equation for the surface space-charge layer, $\Delta\sigma_{sc}$ and $\Delta(R_{Hsc}\sigma_{sc}^2)$ between the two surface structures for the $p(3900\ \Omega\,\mathrm{cm})$- and $n(10\ \Omega\,\mathrm{cm})$-type Si wafers are also shown in the upper columns. These values are opposite in sign to the measured $\Delta\sigma$ and $\Delta(R_H\sigma^2)$. Finally, the values of $\Delta\sigma_{ss}$ and $\Delta(R_{Hss}\sigma_{ss}^2)$ obtained by Eqs. (16) and (17) are listed. In the lower column, the surface-state conductivity σ_{ss} from Ref. 14 and the Hall coefficient R_{Hss} estimated by Eq. (2) using the photoemission Fermi surface data in Ref. 9 are shown. From these data, the calculated values of $\Delta\sigma_{ss}$, $R_{Hss}\sigma_{ss}^2$, and $\Delta(R_{Hss}\sigma_{ss}^2)$ are also shown in the lower column. Compare the values of $\Delta\sigma_{ss}$ and $\Delta(R_{Hss}\sigma_{ss}^2)$ in the upper and lower columns, showing the same sign and order of magnitude between the Hall effect and photoemission measurements.

		Present Hall-effect measurements							From Eqs. (16) and (17)			
Type		σ ($10^{-4}\ \Omega^{-1}$)	$\Delta\sigma$	R_H ($\Omega\ \mathrm{T}^{-1}$)	$R_H\sigma^2$ ($10^{-6}\ \Omega^{-1}\ \mathrm{T}^{-1}$)	$\Delta(R_H\sigma^2)$	$\mu_H(1)$ ($\mathrm{cm}^2/\mathrm{Vs}$)	$\mu_H(2)$	$\Delta\sigma_{sc}$ ($10^{-4}\ \Omega^{-1}$)	$\Delta\sigma_{ss}$	$\Delta(R_{Hsc}\sigma_{sc}^2)$ ($10^{-6}\ \Omega^{-1}\ \mathrm{T}^{-1}$)	$\Delta(R_{Hss}\sigma_{ss}^2)$
p	$\sqrt{3}$	6.0		71	26		430	630				
	$\sqrt{21}$	7.5	+1.5	58	32	+6	440	560	−0.4	+1.9	−1.1	+7.1
n	$\sqrt{3}$	15		26	63		390	870				
	$\sqrt{21}$	19	+3.5	20	69	+6	380	770	−0.4	+3.9	−1.9	+7.9

	Estimated from photoemission data					
	σ_{ss}[a] ($10^{-4}\ \Omega^{-1}$)	R_{Hss} ($\Omega\ \mathrm{T}^{-1}$)	$R_{Hss}\sigma_{ss}^2$ ($10^{-6}\ \Omega^{-1}\ \mathrm{T}^{-1}$)		$\Delta\sigma_{ss}$ ($10^{-4}\ \Omega^{-1}$)	$\Delta(R_{Hss}\sigma_{ss}^2)$ ($10^{-6}\ \Omega^{-1}\ \mathrm{T}^{-1}$)
$\sqrt{3}$	0.75		−39	−0.22		
$\sqrt{21}$	3.2		+11	+1.1	+2.5	+1.3

[a]From Ref. 14.

From the data in Fig. 3, the value of $\Delta(R_H\sigma^2)$ is calculated as $\sim+6\times10^{-6}\ \Omega^{-1}\ \mathrm{T}^{-1}$ for both the p- and n-type wafers, as shown in Table I.

Next we evaluate the surface space-charge-layer contributions, $\Delta\sigma_{sc}$ [Eq. (16)] and $\Delta(R_{Hsc}\sigma_{sc}^2)$ [Eq. (17)] by solving the Poisson equation.[14] Since the surface Fermi level position measured by PES is $\sim$0.12 and $\sim$0.4 eV above the valence-band maximum for the $\sqrt{3}$-Ag and $\sqrt{21}$-(Ag,Au), respectively,[9,18] the value of σ_{sc} decreases in the $\sqrt{3}$-to-$\sqrt{21}$ conversion, $\Delta\sigma_{sc}<0$, because the space-charge layer changes from a p-type accumulation layer to a depletion layer. This is a change opposite to the experimental result $\Delta\sigma>0$, as discussed above. Similarly, the value of $R_{Hsc}\sigma_{sc}^2$ changes as a function of the surface Fermi-level position as shown by the curve in Figs. 4(a) and 4(b) (these results are displayed with respect to the value of $\sqrt{3}$-Ag), and in the $\sqrt{3}$-to-$\sqrt{21}$ conversion it decreases, $\Delta(R_{Hsc}\sigma_{sc}^2)<0$ (shown as *sc* in Fig. 4). This is again opposite to the experimental result $\Delta(R_H\sigma^2)>0$. The exact values are shown in Table I. This ensures that the measured values contain the surface-state components in Eqs. (16) and (17).

Inserting the experimental result $\Delta\sigma$ and the calculated $\Delta\sigma_{sc}$ into Eq. (16), the change in surface-state sheet conductivity $\Delta\sigma_{ss}$ is estimated to be 1.9(±0.5) and 3.9(±1.0) $\times10^{-4}\ \Omega^{-1}$ for the p- and n-type wafers, respectively. These values are similar to those in the previous reports[14,16,18,23] ($\sim2\times10^{-4}\Omega^{-1}$) and also consistent with the values estimated from the photoemission spectroscopy results in Ref. 9.

As shown in Figs. 4(a) and 4(b), $\Delta(R_{Hsc}\sigma_{sc}^2)$ between the $\sqrt{3}$-Ag and $\sqrt{21}$-(Ag,Au) surfaces is calculated to be $\sim-1.1\times10^{-6}\ \Omega^{-1}\ \mathrm{T}^{-1}$ for both the p- and n-type wafers, and then from Eq. (17), $\Delta(R_{Hss}\sigma_{ss}^2)$ is determined to be $\sim+7\times10^{-6}\ \Omega^{-1}\ \mathrm{T}^{-1}$ (shown as *ss* in Fig. 4).

For comparison, we estimate the value of $\Delta(R_{Hss}\sigma_{ss}^2)$ from PES data. We first have put in Table I (lower column) the surface-state conductivity σ_{ss} from Ref. 14 and calculated the surface-state Hall coefficient R_{Hss} by Eq. (2) using the PES data. As mentioned in the Introduction, the value of R_{Hss} for the $\sqrt{3}$-Ag was calculated directly from the electron density of $N_n=1.6\times10^{13}\ \mathrm{cm}^{-2}$, and that for $\sqrt{21}$-(Ag,Au) was calculated from the hole (electron)-like carrier density in the second (third) SBZ of $N_p=4.3\times10^{13}\ \mathrm{cm}^{-2}$ ($N_n=0.4\times10^{13}\ \mathrm{cm}^{-2}$) using the definition of the Hall coefficient in the low-field limit [Eq. (2)]. As a result, the estimation of $\Delta(R_{Hss}\sigma_{ss}^2)$ from the PES data turns out to be $\sim+1.3\times10^{-6}\ \Omega^{-1}\ \mathrm{T}^{-1}$, which is in the same order with that obtained in the present measurement. *This confirms quantitatively that we have succeeded in measuring the surface-state component in the Hall effect.*

Finally, we discuss the influence of the carrier relaxation time τ on the Hall effect. The present results that the carrier behavior changes from electronlike to holelike due to the foldings of bands and Fermi surface is caused by Bragg reflection of Fermi electrons by the newly formed periodicity of $\sqrt{21}\times\sqrt{21}$. But if the carriers are so frequently scattered by defects and/or impurities before the Bragg reflection, such folding effect may not be detected. Thus, the Hall effect may be dependent on the carrier relaxation time. Similar phenomena are known for bulk Group-III metals, such as Al and In. These Group-III metals have three valence electrons in the

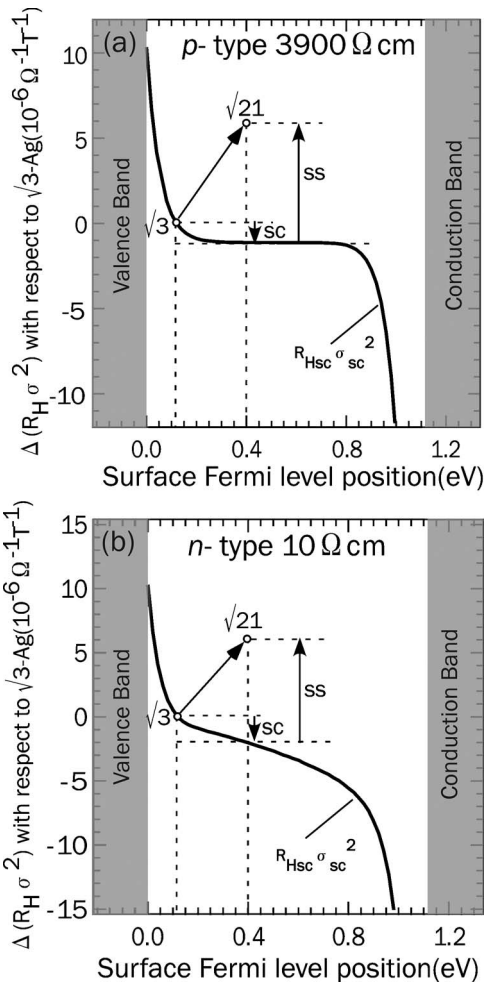

FIG. 4. The measured values of $R_H\sigma^2$ (data points in open circles) for the $\sqrt{21}$-(Ag,Au) with respect to that of the $\sqrt{3}$-Ag. The curve shows the calculated result $R_{Hsc}\sigma_{sc}^2$ for the surface space-charge layer as a function of the surface Fermi level position for *p*-type (3900 Ω cm) (a) and *n*-type (10 Ω cm) (b) Si wafers. *ss*(*sc*) represents the surface-state (space-charge layer) component.

unit cell and possess three-dimensional spherical Fermi surfaces that are slightly larger than the first Brillouin zone. This situation is quite similar to that of the $\sqrt{21}$-(Ag,Au) in two dimension. The Hall coefficients R_H of bulk Al and In are +1 (in charge carrier per unit cell) when the carrier relaxation time τ is enough long and/or the magnetic field B is enough strong, i.e., $\omega_c\tau \gg 1$. But R_H decreases to less than unity for In and −3 for Al with shorter τ and/or weaker B, i.e., $\omega_c\tau \ll 1$.[13,24] This behavior is described in terms of the shape of their Fermi surfaces, and the same mechanism can be applied to the present case of the $\sqrt{21}$-(Ag,Au) as follows. As shown in Figs. 1(e) and 1(f), carriers in the hole pocket in the second SBZ exhibit holelike behavior and those in the third SBZ are electronlike under magnetic field strong enough for electrons to move around the whole Fermi surface before being scattered. However, in the low-field limit, the mean free path of the electrons is much shorter than the real-space trajectory of the Fermi surface; the electrons can only move along short segments on the Fermi surface during the relaxation time. As a result, the Fermi electrons at the hole pocket exhibit both holelike and electronlike behavior, depending on portions of the Fermi contour.[24] For instance, the carriers at point A in Fig. 1(e) are scattered extensively before suffering the Bragg reflection, resulting in an electronlike behavior, whereas those near the cusp at *B* can still undergo the Bragg reflection during their lifetime and behave as holes. The fraction of holelike carriers increases by applying a stronger magnetic field and/or with the longer relaxation time because the trajectory in real space is inversely proportional to the magnetic field,[13] and this is responsible for the R_H change with $\omega_c\tau$ for bulk Al and In.[24] Thus, it is not easy to determine the character of the majority carrier (electronlike or holelike) in the low-field limit. Factors other than the relaxation time that determine their character are the Fermi velocity or the curvature of the trajectory.[24] Since the Fermi velocity is expected to be the same for both the electronlike and holelike carriers, our results for the $\sqrt{21}$-(Ag,Au) seem to indicate that the curvature is essential for the holelike behavior even in the low-field limit; the carriers undergo the Bragg reflection when passing through the cusps *B* in the Fermi surface in the second SBZ, and the holelike contribution becomes likely dominant.

It is noted that R_H of the $\sqrt{21}$-(Ag,Au) can never correspond to three valence electrons as for the case of Al in the low-field limit, as such change would give $\Delta(R_{Hss}\sigma_{ss}^2) < 0$, which is opposite to the present measurement result. In this sense, the present result favors the interpretation that the electrons of $\sqrt{21}$-(Ag,Au) have already undergone the Bragg reflection at the initial state in the photoemission process.[9] Previously, Crain *et al.* have suggested that the electrons feel the $\sqrt{21}\times\sqrt{21}$ superlattice potential when they are emitted from the crystal into the vacuum (final state effect),[12] which is not the case according to our present results.

V. CONCLUSION

We have demonstrated the direct Hall effect in surface states on a semiconductor surface, which is consistent with the electronic structure obtained by photoemission spectroscopy. This surface-state Hall effect motivates further studies on carrier properties at the atomic scale and by utilizing state-of-the-art microscopic four-point probes,[25,26] the present method may be developed into a more surface-sensitive technique. Furthermore, performing measurements at very low temperature will make the bulk contribution negligible and we may be able to succeed in measuring the quantum Hall effect in the 2DEG of an atomic layer by applying a very strong magnetic field.

ACKNOWLEDGMENTS

S. Takeda-Nishino is gratefully acknowledged for her kind help and suggestions. N. Nagamura, K. Motegi, Y. Hamamoto, and Y. Hosomura are gratefully acknowledged for their help during the experiments. This work has been supported by Grants-In-Aid from the Japanese Society for the Promotion of Science.

*Electronic address: matsuda@surface.phys.s.u-tokyo.ac.jp

[1] E. H. Hall, Am. J. Math. **2**, 287 (1879).
[2] H. Ohno, A. Shen, F. Matsukura, A. Oiwa, A. Endo, S. Katsumoto, and Y. Iye, Appl. Phys. Lett. **69**, 363 (1996).
[3] K. v. Klitzing, G. Dorda, and M. Pepper, Phys. Rev. Lett. **45**, 494 (1980).
[4] D. C. Tsui, H. L. Stormer, and A. C. Gossard, Phys. Rev. Lett. **48**, 1559 (1982).
[5] O. Pfennigstorf, A. Petkove, H. L. Guenter, and M. Henzler, Phys. Rev. B **65**, 045412 (2002).
[6] N. G. Galkin, D. L. Goroshko, A. V. Konchenko, V. A. Ivanov, and A. S. Gouralnik, Surf. Rev. Lett. **6**, 7 (1999).
[7] I. Vilfan, M. Henzler, O. Pfennigstorf, and M. Henzler, Phys. Rev. B **66**, 241306(R) (2002).
[8] M. Jalochowski, M. Hoffmann, and E. Bauer, Phys. Rev. Lett. **76**, 4227 (1996).
[9] I. Matsuda, T. Hirahara, M. Konishi, C. Liu, H. Morikawa, M. D'angelo, S. Hasegawa, T. Okuda, and T. Kinoshita, Phys. Rev. B **71**, 235315 (2005).
[10] T. Hirahara, I. Matsuda, M. Ueno, and S. Hasegawa, Surf. Sci. **563**, 191 (2004): T. Hirahara, I. Matsuda, and S. Hasegawa, e-J. Surf. Sci. Nanotechnol. **2**, 141 (2004).
[11] C. Liu, I. Matsuda, R. Hobara, and S. Hasegawa, Phys. Rev. Lett. **96**, 036803 (2006): Y. Nakajima, G. Uchida, T. Nagao, and S. Hasegawa, Phys. Rev. B **54**, 14 134 (1996).
[12] J. N. Crain, K. N. Altmann, C. Bromberger, and F. J. Himpsel, Phys. Rev. B **66**, 205302 (2002).
[13] N. W. Ashcroft and N. D. Mermin, *Solid State Physics* (Saunders College, New York, 1976), Chap. 9, 14.
[14] S. Hasegawa, X. Tong, S. Takeda, N. Sato, and T. Nagao, Prog. Surf. Sci. **60**, 89 (1999).
[15] P. Blood and J. W. Orton, *The Electrical Characterization of Semiconductors: Majority Carriers and Electron States* (Academic, New York, 1992).
[16] S. Hasegawa and S. Ino, Phys. Rev. Lett. **68**, 1192 (1992).
[17] I. Matsuda, M. Ueno, T. Hirahara, R. Hobara, H. Morikawa, C. Liu, and S. Hasegawa, Phys. Rev. Lett. **93**, 236801 (2004).
[18] X. Tong, S. Hasegawa, and S. Ino, Phys. Rev. B **55**, 1310 (1997).
[19] In the Hall resistance, some contribution from the longitudinal resistance may be included because we cannot place the Hall-voltage probes completely perpendicular to the current flow. But the linear dependence in R_{Hall}-B curves in Figs. 3(c)–3(e) shows that the longitudinal component is very small and can be neglected because, as discussed in the text, the longitudinal component should have a parabolic dependence to the magnetic field. Furthermore, we can experimentally delete the contribution of the longitudinal voltage drop by reversing the direction of magnetic field.
[20] R_H is positive even for the n-type wafer because the surface space-charge layer is p-type. Because of the formation of a p-n junction in the subsurface region between the surface space-charge layer and the interior bulk, the current does not flow into the bulk and the main contribution comes from the space-charge layer.
[21] C. Hamaguchi, *Basic Semiconductor Physics* (Springer-Verlag, Berlin, 2001).
[22] S. M. Sze, *Physics of Semiconductor Devices* (Wiley, New York, 1981), Chap. 1.
[23] C.-S. Jiang, X. Tong, S. Hasegawa, and S. Ino, Surf. Sci. **376**, 69 (1997).
[24] C. M. Hurd, *The Hall Effect in Metals and Alloys* (Plenum Press, New York, 1972), Chap. 3, and references therein.
[25] T. Kanagawa, R. Hobara, I. Matsuda, T. Tanikawa, A. Natori, and S. Hasegawa Phys. Rev. Lett. **91**, 036805 (2003).
[26] T. Tanikawa, I. Matsuda, T. Kanagawa, and S. Hasegawa, Phys. Rev. Lett. **93**, 016801 (2004).